Young's modulus of elasticity of Schlemm's canal endothelial cells

Dehong Zeng,
Department of Biomedical Engineering, Northwestern University, Evanston, USA

Taras Juzkiw,
Department of Mechanical and Industrial Engineering, University of Toronto, Toronto, Canada

A. Thomas Read,
Department of Mechanical and Industrial Engineering, University of Toronto, Toronto, Canada

Darren W.-H. Chan,
Department of Mechanical and Industrial Engineering, University of Toronto, Toronto, Canada

Matthew R. Glucksberg,
Department of Biomedical Engineering, Northwestern University, Evanston, USA

C. Ross Ethier, and
Department of Mechanical and Industrial Engineering, University of Toronto, Toronto, Canada.
Institute of Biomaterials and Biomedical Engineering, University of Toronto, Toronto, Canada.
Department of Bioengineering, Imperial College London, London, UK

Mark Johnson
Department of Biomedical Engineering, Northwestern University, Evanston, USA

Mark Johnson: m-johnson2@northwestern.edu

Abstract

Schlemm's canal (SC) endothelial cells are likely important in the physiology and pathophysiology of the aqueous drainage system of the eye, particularly in glaucoma. The mechanical stiffness of these cells determines, in part, the extent to which they can support a pressure gradient and thus can be used to place limits on the flow resistance that this layer can generate in the eye. However, little is known about the biomechanical properties of SC endothelial cells. Our goal in this study was to estimate the effective Young's modulus of elasticity of normal SC cells. To do so, we combined magnetic pulling cytometry of isolated cultured human SC cells with finite element modeling of the mechanical response of the cell to traction forces applied by adherent beads. Preliminary work showed that the immersion angles of beads attached to the SC cells had a major influence on bead response; therefore, we also measured bead immersion angle by confocal microscopy, using an empirical technique to correct for axial distortion of the confocal images. Our results showed that the upper bound for the effective Young's modulus of elasticity of the cultured SC cells examined in this study, in central, non-nuclear regions, ranged

Correspondence to: Mark Johnson, m-johnson2@northwestern.edu.

between 1,007 and 3,053 Pa, which is similar to, although somewhat larger than values that have been measured for other endothelial cell types. We compared these values to estimates of the modulus of primate SC cells in vivo, based on images of these cells under pressure loading, and found good agreement at low intraocular pressure (8–15 mm Hg). However, increasing intraocular pressure (22–30 mm Hg) appeared to cause a significant increase in the modulus of these cells. These moduli can be used to estimate the extent to which SC cells deform in response to the pressure drop across the inner wall endothelium and thereby estimate the extent to which they can generate outflow resistance.

Keywords

Magnetic bead pulling cytometry; Immersion angle; Cell stiffness; Glaucoma

1 Introduction

Glaucoma describes a group of potentially blinding ocular disorders. Recent work estimates that worldwide there will be approximately 60.5 million people with glaucoma in 2010, increasing to 79.6 million by 2020; of these, 8.4 million will be bilaterally blind by 2010, increasing to 11.2 million by 2020 (Quigley and Broman 2006). The primary risk factor for the development of vision loss in glaucoma is elevated pressure within the eye (intraocular pressure, or IOP), and lowering of IOP is currently the only therapeutic option with proven efficacy (Kass et al. 2002). IOP is generated as aqueous humor drains out of the eye against the hydrodynamic resistance of a series of specialized tissues. Most causes of elevated IOP leading to glaucoma are due to an increase in flow resistance of these tissues, and there is therefore great interest in understanding the biomechanics of aqueous humor drainage.

Experimental evidence implicates the juxtacanalicular connective tissue (JCT) and/or the inner wall endothelium of Schlemm's canal as the major site(s) of aqueous humor outflow resistance (Maepea and Bill 1992; Johnson 2006) in the eye (see Fig. 1 for anatomy and terminology). Aqueous humor is thought to cross from the JCT to the lumen of Schlemm's canal through pores in the inner wall endothelium, and there are fewer of these pores in eyes with primary open angle glaucoma (POAG) than in normal eyes (Allingham et al. 1992; Johnson et al. 2002). Moreover, Schlemm's canal endothelial cells undergo large mechanical deformations as IOP changes (Ethier 2002), forming structures (giant vacuoles) that are thought to be involved in aqueous humor passage. This indicates that there is a transcellular pressure drop across the inner wall endothelium, making the biomechanics of these cells of great interest.

The biomechanical situation of SC cells is different from that of vascular endothelium, which is subject to a pressure gradient in the apical to basal direction. The connective tissue underlying vascular endothelium can support the load generated by this gradient, and thus vascular endothelial cells do not have to support the entire radial and circumferential loads generated by lumenal pressure. This is not the case for the endothelium of Schlemm's canal, since the aqueous humor flows in a basal to apical fashion leading to a pressure gradient in the opposite direction from that for vascular endothelium. Thus, SC cells must directly support a transcellular pressure difference, suggesting that the flow resistance of this layer

may be small and limited by its mechanical strength. This appears to be inconsistent with the work of some groups, who have proposed that this cellular lining is directly responsible for generating a significant fraction of outflow resistance (Underwood et al. 1999; Burke et al. 2002; Alvarado et al. 2005).

Based upon these considerations, the mechanical properties of the cells of the inner wall of Schlemm's canal are likely important in aqueous humor drainage, and the stiffness of these cells, particularly an upper bound of this stiffness, is important to determining a limit on the flow resistance that SC endothelium might generate. Thus, our goal in this work is to measure the mechanical stiffness of SC inner wall cells in human eyes with emphasis on finding an upper bound. The results will be used in later studies to determine how large of a pressure drop can be supported across the inner wall of Schlemm's canal.

2 Materials and methods

2.1 Overview

A variety of techniques are available for measuring cellular stiffness, including atomic force microscopy (Sato et al. 2004; Schrot et al. 2005; Costa et al. 2006), micropipette aspiration (Deguchi et al. 2005), optical trapping (Henon et al. 1999), microplate compression (Caille et al. 2002), and magnetic bead twisting/pulling (Wang and Ingber 1995; Laurent et al. 2002; Karcher et al. 2003; Feneberg et al. 2004; Matthews et al. 2004; Overby et al. 2005). In this study, we used magnetic bead pulling due to its reliability and comparative simplicity. Paramagnetic beads coated with RGD peptide were bound to sub-confluent SC cells. A magnetic force of 800 pN was applied by a micro-needle for 3–4 s during which time movement of the beads were recorded through videomicroscopy (see Fig. 2). Displacements of the beads as a function of time were obtained by analyzing the videomicroscopy images.

To estimate an effective Young's modulus of elasticity of the SC cells from the results of these experiments, we used a finite element model to simulate the displacement of a magnetic bead attached to a cultured SC cell. We estimated the modulus of the cell by finding the value that best matched the model predictions to the experimental data. Bead displacements in our numerical simulations strongly depended on the depth to which the magnetic bead embedded in the cell, and thus fluorescence microscopy was used to estimate the depth of bead immersion.

2.2 Cell culture

Human SC cells were harvested from both eyes of a normal human donor (76-year-old male) supplied from the National Disease Research Interchange (Philadelphia, PA) within 40 h post-mortem, using a CD31 immunopanning technique as described by Karl et al. (2005). The SC cells were plated on 60 mm culture dishes (product# 83-1801, Sarstedt, Montreal, Canada) and cells in each dish were maintained in 5 ml of DMEM with low glucose supplemented with 10% fetal bovine serum (FBS), penicillin (100 unit/ml), streptomycin (100 μg/ml), and L-glutamine (292 μg/ml). The medium was changed daily. The cells were passaged at confluence with a 1:12 split ratio (around 4×10^4 cells/ml).

Unlike trabecular meshwork cells, SC cells express the von Willebrand factor–receptor complex (vWF) (Stamer et al. 1998). Cells were tested for presence of vWF using immunofluorescence to confirm that they were SC cells. The primary antibody was rabbit anti-human (1:200 dilution, Sigma) and the secondary antibody was fluorescein isothiocyanate-conjugated goat anti-rabbit IgG (1:1,000 dilution, Biosource). Cultured cells showed positive labeling, confirming that they were in fact SC cells.

2.3 Magnetic pulling cytometry

2.3.1 Magnetic beads—We generally followed the methods for magnetic bead pulling cytometry as described by Matthews et al. (2004). We used 4.5 μm diameter superparamagnetic, tosyl-activated Dynabeads (product#140.13, Dynal Biotech, Brown Deer, USA). These polystyrene beads have a polyurethane layer embedded with p-toluenesulphonyl (tosyl) reactive groups. The beads contained iron oxide in the form of maghemite (γ-Fe_2O_3) that gave them their superparamagnetic qualities.

To promote specific attachment of the beads to the cells, a synthetic peptide (Peptite-2000, Integra LS, San Diego, USA) that contains the Arg-Gly-Asp (RGD) sequence was adsorbed hydrophobically onto the bead. 100 μl of bead solution and 10 μl of the peptide at a concentration of 50 μg/ml were added to 900 μl of 0.1M sodium carbonate buffer (pH 9.4). The solution was rotated in an end-over-end rotator for 24 h at 4°C. The coated beads were washed twice in PBS and then stored in PBS at 4°C at concentration of 2×10^6 beads/100 μl (Wang et al. 1993).

2.3.2 Magnetic needle and magnetic force calibration—A magnetic microneedle assembly was the source of the magnetic field gradient used to pull the microbeads attached to the cells. The magnetic microneedle assembly consisted of a 5-cm long stainless steel sewing needle glued to the top of a permanent neodymium iron boron (NeFeB) disc magnet (26 mm in diameter, 6 mm in height; Edmund Industrial Optics) that was in turn glued to an aluminum rod (1.25 cm in diameter, 15 cm in length). This assembly was mounted onto an electric micromanipulator (MP-285, Sutter Instruments, California, USA) at an angle of 30° from the horizontal.

The magnitude of the horizontal magnetic force applied to each bead was a function of the distance between the needle tip and the bead. To calibrate the magnetic force, single beads were placed in a 100% glycerol solution (BDH, Ana-laR; VWR Scientific) near the needle, and bead motion was tracked by video microscopy. The temperature of the glycerol was measured with a thermocouple, allowing the viscosity of the glycerol to be calculated from standard tables (Gilmont 2002). The instantaneous horizontal velocity of single beads was obtained through analyzing video microscopic images, and the viscous force on a bead was calculated based on Stokes Law (Yih 1988):

$$F = 6\pi \mu R U \quad (1)$$

where F was the total viscous force on the bead, μ the dynamic viscosity of the glycerol, R the bead radius, and U the bead velocity. Magnetic force decayed as a function of distance

from the needle tip. The calibration was performed eight times, and the force versus distance data were regressed to an exponential equation (Fig. 3).

2.3.3 Videomicroscopy—The motions of the beads were imaged using a Zeiss Axiovert 200 (Carl Zeiss, Jena Germany) motorized inverted microscope equipped with a MS1000 camera (Canadian Photonics Laboratory Inc., Minnedosa, Canada). The microscope was mounted on a 63–500 series TMC (Technical Manufacturing Corporation, Peabody, USA) air isolation table. The camera was fitted with a 2× expanding lens (2-EX C80001, Cosmicar/Pentax) to image the region around a bead, with a spatial resolution of 0.1025 μm/ pixel at a recording rate of 200 frames per second. A Hamamatsu ORCA ER camera (Bridgewater, USA) was also mounted to the microscope to acquire high-resolution still images of cells and beads for locating the bead to be pulled. During a bead pulling experiment, the temperature of the culture dish was maintained at 37°C by a Zeiss POC-R culture dish heater that was fitted onto the microscope stage.

IPLab (v3.65, Scanalytics, Fairfax, USA) was used to control the motorized elements of the microscope and acquire the still images. Image acquisition by the MS1000 camera was controlled by proprietary software from Canadian Photonics Laboratory (Minnedos, Canada). The high-speed logger VI in Labview (v6.1, National Instruments) was used to record the voltage outputs of the camera and the micromanipulator in order to synchronize image acquisition with micro-needle motion.

2.3.4 Magnetic bead pulling experiment—SC cells in their fourth or fifth passages were grown until they were 50–60% confluent before being used for bead pulling experiments. Prior to bead pulling, cells were serum starved for 18–20 h to hinder cell migration, synchronize cells at G0 in the cell cycle, reduce serum-dependent pre-stress levels, and standardize the experimental conditions (Wang and Ingber 1995).

Suspended beads prepared as described above were sonicated with a Wand sonicator (Kontes probe sonicator, Vineland, New Jersey) for 3 s at low power to disperse any clumps and were then added to the cells in a concentration that allowed attachment of one to two beads per cell, typically 100 μl of bead solution at 2×10^5 beads/100 μl. An example of a bead bound to a cell is shown in Fig. 4a. The cells with beads were incubated for 10 min at 37°C to enhance attachment, then unbound beads were washed away with PBS and the dish was topped up with 5 ml of serum-free medium. During the bead pulling experiment, the distance between the bead and the needle tip was directly measured on the Live Image Preview window of the IPLab software.

A cell with one or two beads attached was first identified using the ORCA camera. The tip of the micro-needle was placed 200 μm away from the bead to be pulled and vertically positioned such that the needle tip was in the same horizontal plane (within 2 μm or less) as the center of the bead (based on object focus). Typically the needle tip was 5–15 μm off the floor of dish, and a phase-contrast image was then taken to record the cell shape and bead location before the experiment. The data acquisition program was started to record the camera and micromanipulator outputs. The MS1000 camera was started to capture image frames and the micromanipulator was set into motion. The micro-needle tip was moved

towards the bead at a speed of 2,545 μm/s and stopped after 0.055 s at a location 60 μm away from the bead for 4 s, exerting a horizontal force of approximately 800 pN on the bead. The micro-needle was then moved away from the bead to a distance of 200 μm. The above manipulation was repeated twice on each bead before the image acquisition was stopped.

The needle tip was then manually moved up about 400 μm from the bottom of the dish to avoid interaction with neighboring cells while the next bead was being found. Once the next bead was found, the needle tip was brought back down and the whole procedure was repeated. The experiment was completed within 1 h.

Two in-house Matlab (v6.5 R13, MathWorks, Natick, USA) programs were used to analyze the images to determine the motion of the centroid of the bead caused by the magnetic force and hence deduce the displacement of the bead center as a function of time (Overby et al. 2005). Such methods allow nanometer resolution for determining bead location (Gelles et al. 1988; Cheezum et al. 2001). Measured bead displacement data were regressed (KaleidaGraph, version 3.6, Synergy Software, Reading, PA, USA) to the following visco-elastic response model:

$$s = s_\infty - \left(s_\infty - s_0\right) e^{-\frac{t}{\tau_0}} \quad (2)$$

to obtain the long-time displacement s_∞, the initial displacement s_0, and the relaxation time constant τ_0. s_0 is a measure of the stiffness of the elastic components of a cell (Ethier and Simmons 2007) and hence we focused on this parameter in our finite element modeling studies (see below) to obtain an upper bound on SC cell stiffness. This bound may eventually be important for understanding the maximum pressure loading that inner wall cells can support (Ethier et al. 2008). For completeness, we also estimated the SC cell stiffness that resulted from fitted values of s_∞.

2.3.5 Order of magnitude analysis—It is important to understand that the parameters s_∞ and s_0 obtained by fitting bead displacement data to Eq. (2) give only an indirect measure of cell stiffness. To obtain Young's modulus of elasticity values, additional steps are required. Here we perform an order of magnitude analysis to estimate Young's modulus for SC cells. This analysis guided the selection of an appropriate parameter range for Young's modulus for use in finite element parametric studies described below. It was also a necessary material parameter input for mesh dependency tests for the finite element model.

Considering purely elastic deformation, the work done by the magnetic force on a bead is converted to elastic strain energy in the cell surrounding the bead (Fung 1977), i.e.

$$\vec{F} \cdot \vec{s} \quad \iiint \tfrac{1}{2} \sigma_{ij} \varepsilon_{ij} dv \quad i, j = 1, 2, 3 \quad (3)$$

where $\vec{F}$ and $\vec{s}$ are the magnetic force acting on the bead and the displacement of the bead center, respectively, and σ_{ij} and ε_{ij} are the deviatoric stress and deviatoric strain tensors in the surrounding cell, respectively. The volume integration is over the region of the cell

deformed by the bead pulling, which we roughly estimate as twice the volume of the bead. By considering the order of magnitude of each term in the above equation for a linearly elastic and isotropic material, i.e. a material for which $\sigma_{ij} = \frac{E}{(1+v)}\varepsilon_{ij}$ (Fung 1977), where E is Young's modulus of the cell and v is the Poisson ratio, we can write

$$2Fs \sim EV\varepsilon^2 \quad (4)$$

where V is the volume of the cell mechanically influenced by the bead pulling and we set $v = 0.5$ assuming incompressibility of the cell. If we further assume that the deformation volume was proportional to the volume of the bead with constant of proportionality k, i.e., $V \sim \frac{4}{3}k\pi R^3$, and the magnitude of strain was $\varepsilon \sim \frac{s}{R}$, where $R = 2.25$ μm is the radius of the bead, then we can write

$$E \sim \frac{9F}{4k\pi\, Rs} \quad (5)$$

The above equation was convenient for estimating the order of magnitude of Young's modulus of SC cells based on magnetic force, bead displacement, and bead radius. By substituting the pulling force $F = 800$ pN, and using a typical displacement of $s \approx 0.1$μm and assuming that the cell volume influenced by the displacement of the bead is roughly twice the volume of the bead ($k = 2$), we obtained an estimate of 1000 Pa for the Young's modulus of these cells.

2.4 Determination of bead half-immersion angle

When beads attach to a cell, they become partially embedded in the cell (Laurent et al. 2002). Studies using magnetic bead twisting/pulling have shown that displacement of a bead embedded in a cell strongly depends on (1) half immersion angle of the bead and (2) the distance from the bottom of the bead to the basal surface of the cell (Laurent et al. 2002; Mijailovich et al. 2002; Karcher et al. 2003; Ohayon et al. 2004; Ohayon and Tracqui 2005).

Consider a coordinate system such that base of the cell is parallel to the xy plane and the z axis points from the cell's basal surface to its apical surface. The half immersion angle (α) is defined as the half angle of the cone formed by the bead center and the contact line of the bead with the cell's surface (Fig. 5, left panel). Let z_a and z_c be the height (z coordinate) of the apical surface and bead center, respectively. Then, α can be found as:

$$\alpha = \frac{\pi}{2} - \arcsin\left(\frac{z_c - z_a}{R}\right) \quad (6)$$

To determine α, we conducted fluorescent confocal microscopic studies on beads attached to SC cells. Briefly, 4 μm blue fluorescent FluoSpheres (Molecular Probes, Eugene, Oregon) coated with RGD synthetic peptide (Peptite-2000, Integra LS, San Diego, USA) in the manner as the magnetic beads were added to passage 4, 40–60% confluent SC cells that were harvested from a 53 year old human donor eye (courtesy of Dr. Daniel Stamer,

University of Arizona). These cells were then labeled with PKH26 membrane label, a vital stain for cell membrane labeling (Sigma # MINI26, PKH26 Red Fluorescent Cell Linker Kit). After the beads were attached to the cells, the cells were fixed with 2% formalin in PBS for 20 min, and then stored in 1% formalin. The total time for bead-cell exposure, binding and fixation of cells was less than 1 h.

Confocal images of beads and the cytoplasm surrounding the bead were obtained using a Zeiss LSM510 Meta Confocal Laser Scanning Microscope (Carl Zeiss, Inc., Germany) and the confocal images were deconvolved to improve image resolution using AxioVision (release 4.6, Carl Zeiss, Inc., Germany). Confocal images of a bead and its surrounding cytoplasm were collected by optically sectioning from the top of the bead to the basal surface of the cell, to obtain a z-stack of image slices with each slice being parallel to the xy plane (basal surface). The scanning z-step was $z = 0.2$ μm, with an in-plane resolution of 0.06–0.15 μm/pixel.

The fluorescent images suffered from axial distortion, a common problem with fluorescent images (Ferko et al. 2006), causing the image of a spherical bead to be distorted into an ellipsoid (see schematic in Fig. 5, right panel). This resulted in inaccurate measurements of the height of the apical cell surface and bead center. We adopted the empirical approach of Ferko et al. (2006) to correct axial distortion of the image.

There was little in-plane image distortion, i.e. in the x or y directions. For example, the nominal bead diameter specified by the manufacturer was 4.0 ± 0.14 μm, and the maximum section diameters directly measured from the confocal images in the x- and y-directions were 4.11 ± 0.13 μm and 4.08 ± 0.13 μm, respectively (mean $\pm$ SD; $n = 14$), confirming that the image distortion in x and y directions were indeed negligible and that correction was necessary in the z-direction only.

Since the cell membrane was labeled, we defined the apical surface ($z = z_a'$) of the cell to be the location of the image slice within the confocal image stack having peak fluorescence intensity of the membrane, with the fluorescence intensity measured as a function of the z coordinate using ImageJ (1.38X, NIH, USA). The section diameter D_a of the bead at this same location ($z = z_a'$) was measured from the relevant image slice, (Fig. 5, right panel). We then considered a spherical bead centered at the same location as the distorted bead (at $z = z_c$). We determined the corrected height (z_a) at which the section diameter of this spherical bead was D_a by using Eq. (7) (Ferko et al. 2006)

$$\begin{aligned} z_a = z_c + \sqrt{R^2 - D_a^2/4} \quad & z_a > z_c \\ z_a = z_c - \sqrt{R^2 - D_a^2/4} \quad & z_a \leq z_c \end{aligned} \quad (7)$$

We then used the corrected value of z_a to compute a from Eq. (6).

2.5 Finite element modeling

2.5.1 Model of cell with bead—Finite element modeling allows deformations and stresses in a solid body to be computed if the geometry, boundary conditions and material

properties of the deforming bodies are known, or conversely, as we do in this study, to estimate the material properties if the deformations and geometry are know. Magnetic cytometry can be combined with finite element models to estimate cellular mechanical properties (Mijailovich et al. 2002). We modeled beads that were at least 10 μm away from the cell edge, and were not close to the nucleus, as shown in Fig. 4a, to exclude the influence of the nucleus and the dense actin filament network at the edge of the cell (see Fig. 4b) (Ethier et al. 2004). A previous study on magnetic beads attached to NIH 3T3 fibroblasts indicated that the stress and strain induced by pulling a 4.5 μm bead were localized to a region of not more than 10 μm away from the bead (Karcher et al. 2003). Similarly, Bausch et al. estimated that the radius of influence around a magnetically perturbed 4.5 μm bead was less than 7 μm (Bausch et al. 1998). This was consistent with our initial studies, in which we modeled approximately one quarter of a cell containing a bead, and found that the strain had dropped to 0.1% at a radius of 10 μm from the bead center as compared to roughly 10% near the bead (Zeng et al. 2007). For the work reported herein, we therefore restricted the computational domain so that it consisted of a bead bound to a cell and a cylindrical cytoplasmic region within 10 μm of the bead center (Fig. 6). No significant differences were seen between the results from this model and those using a larger domain.

In these simulations, the apical surface of the cell was modeled as horizontal, implying constant cell thickness; however, in reality, cell thickness decreased as the cell periphery was approached. We used the confocal images to estimate the slope of the apical surface towards the cell periphery, and found it to be roughly 0.05. To examine the influence of this slope on our results, we conducted one simulation in which the slope of the apical surface was set to 0.1, and compared the predicted bead displacement against that of a horizontal apical surface. The difference in bead displacement was only 1.5%, leading to no appreciable influence on our estimates of cell modulus.

We modeled the cell as having a uniform modulus of elasticity and did not consider separately the cell membrane, cortex and cytoskeleton. As such, the modulus that we determined was an aggregate quantity. The bead was modeled as a rigid body due to its having a much higher stiffness than the cell, and the bead was assumed fixed to the cell at their mutual interface. The cell was modeled as a linearly elastic material. Zero radial and axial displacement boundary conditions were imposed at the basal surface of the cell and the cylindrical side surfaces of the domain, while a zero stress boundary condition was placed on the apical surface that was not in contact with the bead. A horizontal traction force of 800 pN was applied at the bead center.

The finite element model was developed using ABAQUS CAE/Standard (Version 6.7, ABAQUS Inc., Providence, RI, USA). We used 8-node hexahedral elements to discretize the cell, and there were typically 80,000 nodes in one model. Solution times were typically 900 seconds. A mesh refinement study was performed by using successively refined hexahedral meshes with nodal spacing of $h = 0.6, 0.3, 0.15$ μm. In these mesh refinement studies, Young's modulus of elasticity was assumed to be 1,000 Pa based on the result of the order of magnitude analysis described above. Compared to the solution from the most refined mesh (nodal spacing 0.15 μm), displacement at the bead center obtained from meshes with $h = 0.6$ and 0.3 μm differed by 5 and 1.4%, respectively, confirming that the

solution could be considered converged when the mesh was refined to $h = 0.3$ μm, which was the refinement used for all simulations reported here.

Our goal was to determine bounds for the modulus of these SC cells. We did this in a two-step procedure. We first performed parametric studies on the effects of cell thickness ranging between a minimum value (see below) and 10 μm while using a Young's modulus of elasticity of 1,000 Pa in combination with each of the measured minimum, average, and maximum bead immersion angles. More specifically, the minimum cell thickness value was 1.5 μm for simulations done with the minimum measured immersion angle, 2.5 μm for simulations with the average measured immersion angle, and 3 μm for simulations with the maximum measured immersion angle. This variation was necessary due to differences in bead embedding depth and also difficulties with mesh generation in the cytoplasm near the bottom of the bead for thin cells. The outcome measure of these studies was computed bead displacement.

This first step allowed us to determine that using the minimum half immersion angle and maximum cell thickness would lead to the maximum estimate for modulus (the upper bound case). Similarly, using the maximum half immersion angle and minimum cell thickness would lead to the minimum modulus estimate (the lower bound case). Importantly, these studies indicated that there was little difference in predicted bead displacement when cell thickness was changed from 5 to 10 μm, which justified 10 μm as the maximum cell thickness we investigated.

In the second step, we performed parametric studies in which we varied the cellular Young's modulus of elasticity, compared measured bead displacements with the calculated bead displacements, and adjusted Young's modulus to match simulation results to the measurements. The value of the Young's modulus that gave the best match was taken as the actual modulus of the cell. This procedure was done for both the upper and lower bound cases, thus yielding a range of Young's modulus of elasticity for SC cells.

3 Results

3.1 Experimental measurements

The displacements of 12 beads attached to 10 SC cells were measured. A typical bead displacement response during a magnetic bead-pulling experiment is shown in Fig. 7. There was an elastic response corresponding to the initial jump in displacement, followed by viscoelastic creep. We determined a best fit to these data using the regression techniques described above (Table 1). Typically smaller displacements were seen for beads attached near the periphery of the cell or near the nucleus as compared to those at other locations.

To measure bead half immersion angles, 14 beads attached to SC cells, at least 10 μm away from the cell edge, were examined using confocal microscopy. The half immersion angles were 84° ± 11.7° (mean ± SD) with a minimum of 60° and a maximum of 100° (see Fig. 8). Most beads were imbedded with half-immersion angles between 80° and 100°. The uncertainty of measurement of this angle ranged between 14° and 18° due to the uncertainty (±0.5 μm) in determining the location of the apical surface of the cell.

3.2 Simulations

Figure 9 shows the results of numerical studies conducted to determine the sensitivity of predicted bead displacement to the thickness of the cytoplasm at the bead embedding site (since this parameter was not measured). The predicted displacements (s) were found to depend on cell thickness (w) according to an exponential function of the form $s = A - Be^{-w/C}$, where A, B, and C were constants. Values of C were found to be 1.29, 2.15 and 2.22 μm for the minimum, average, and the maximum half immersion angles, respectively (correlation coefficients of 0.9996, 0.985, and 0.984). These results indicated that for cytoplasmic thicknesses greater than approximately 5 μm, the predicted bead displacement was insensitive to cytoplasmic thickness.

We then calculated bead displacements for the upper bound (half immersion angle of 60° and cell thickness 10 μm) and lower bound (half-immersion angle of 98° and cell thickness of 3 μm) cases. Figure 10 shows the two curves that result for these two bounding cases. By adjusting the cell modulus such that the measured bead initial displacement is matched to the upper bound curve, an upper bound estimate of the modulus of this cell was obtained. A similar procedure was used to establish a lower bound. An example is shown for cell 2. We used this procedure for the initial displacement of each bead (s_0) to place bounds on the initial displacement modulus (E_0), and used the long time displacement (s_∞) to place bounds on E_∞. The results are shown in Table 1.

We estimated that the upper bound on E_0 for beads attached in the central, non-nuclear regions of SC cells ranged between 1007 and 3053 Pa. We also estimated the moduli for perinuclear and peripheral regions of the SC cells and found the values in these regions to be considerably higher. Note that we did not separately model the bead motion in such regions, nor did we do studies to separately examine the depth of bead embedding in these regions. Nonetheless, determination of the moduli of the cell attached to beads in these peripheral and nuclear regions allowed relative comparisons with the remainder of the cell.

A similar procedure, but using the measured long-time bead displacements (s_∞) gave a range of 149–260 Pa for the lower bound estimates of E_∞ for beads attached to SC cells in central, non-nuclear regions. The values were again higher in the periphery and near the nucleus than in the remainder of the cell.

In all cases, the mechanical influence of the bead pull was limited to the near vicinity of the bead, extending about 3 μm from its edge (e.g. Fig. 11). There was considerable difference in local strain pattern between the shallow and deep immersion angles. At the minimum immersion angle, deformations were concentrated near the apical surface in contact with the bead (Fig. 11, panel a). At the maximum immersion angle, maximum deformations shifted to the basal side of the cell, near the bottom of the bead (Fig. 11, panel b).

3.3 In vivo estimates

We next considered the possibility that SC cells, when subjected to physiological loads, may exhibit different mechanical properties than they do in culture, where they are essentially unloaded. We examined data from Grierson and Lee (1977), who characterized the change in volume of giant vacuoles in SC cells of live primate eyes as a function of perfusion

pressure. Giant vacuoles (see Fig. 12) are outpouchings of SC cells thought to be caused by the pressure drop across the inner wall endothelium (Johnson 2006). By assuming these structures behave as thin-shelled spheres under the influence of the transcellular pressure drop, we can use the Grierson and Lee measurements to make a crude estimate of the modulus of these cells in vivo.

A force balance on a thin-shelled sphere whose radius (R) is much greater than its wall thickness (δ) combined with the constitutive law relating deviatoric strain to deviatoric stress (Fung 1977), with the hoop component of this strain defined as $\varepsilon_\theta = (R - R_0)/R$ (Oden 1967), yields the following relationship:

$$E = \frac{R^2 \Delta P}{2\delta(R - R_0)} \quad (8)$$

where R_0 refers to reference conditions at zero pressure drop (P) across the wall of the sphere.

We applied this equation to data from Grierson and Lee for the volume of giant vacuoles as a function of P across the vacuole wall to estimate the modulus of SC cells. Consistent with the data reported by Grierson and Lee, we computed an effective radius of the vacuole from the reported giant vacuole volume data using the formula $V = 4/3\pi R^3$. R_0 was the radius of the vacuole at an IOP of 8 mm Hg. Since P was not directly measured in the original experiments, we considered two cases: (i) the transcellular pressure drop was 10% of the pressure drop (IOP—episcleral venous pressure) across the entire outflow pathway, consistent with the current conventional wisdom (Bill and Svedbergh 1972; Johnson 2006), and (ii) the entire pressure drop occurred across SC endothelium. The thickness ($\delta = 0.13$ μm, mean of 13 images) of the vacuole wall in Schlemm's canal was measured from images of Grierson and Lee (1975). We also considered two cases for the thickness of the vacuole wall: we allowed it to remain constant as IOP increased, or we assumed that the volume of the vacuole wall remained constant, so that δ decreased as the vacuole radius increased.

The data could not be fit with a single value of the modulus, which we attributed to a nonlinear stiffening of the cells as their deformation increased with increasing IOP. As a result, we considered three IOP ranges: 8–15, 15–22 and 22–30 mm Hg, and calculated a value of E for each range using Eq. (8). The results of these calculations are shown in Table 3. If we assumed that transcellular pressure drop across the SC cells was 10% of the total pressure drop, we found that at low IOP, the calculated modulus of the SC cells in these primate eyes showed reasonably good agreement with the values we found in human SC cells in culture. However, if we assumed that the entire pressure drop across the outflow pathway was supported by these cells, very high modulus values were obtained that are inconsistent with our modulus measurements in cultured cells and previous measurements on other cell types (Table 2).

4 Discussion

Schlemm's canal endothelial cells have a relatively unique physiological requirement to support a basal to apical pressure gradient. The extent to which these cells can support such

a load limits the flow resistance that this cell layer can generate under physiologic conditions. This suggests that the Young's modulus of these cells is of considerable physiological importance since the bulk of aqueous humor outflow passes through this endothelium. In particular, an upper bound for the stiffness of these cells will allow an evaluation of the maximum pressure drop that this layer can support, and thereby allow a determination of the maximum flow resistance that this tissue might generate under physiologic conditions. As the precise localization of the principal site of aqueous humor outflow resistance is unknown and is of importance to the understanding of the pathogenesis of glaucoma, the goal of the current study was to determine an upper bound for the Young's modulus of Schlemm's canal cells.

We examined the modulus of these cells in their periphery, in the perinuclear regions, and in central, non-nuclear regions. The latter measurements are likely most important for determining overall capacity of these cells to support a pressure gradient as cell failure will be determined by the cell's weakest aspect. We found that the nuclear and peripheral aspects of cells were typically stiffer than the remainder of the cell (Table 1), in agreement with findings in other endothelial cell types (Caille et al. 2002; Kataoka et al. 2002; Mathur et al. 2007). We found that in the central, non-nuclear regions of the cells, the upper bound for the modulus of these cells was in the range of 1,007–3,053 Pa.

The question arises as to whether SC cells, due to their relatively unique physiological requirements, have higher stiffness as compared to other endothelial cell types. Table 2 shows typical values for Young's modulus in other endothelial cell types. Atomic force microscopy (AFM) gives higher values for cell stiffness (average ~ 3,000 Pa), as compared with other methods such as magnetic twisting cytometry, micropipette and microplate (average ~ 400 Pa). Of these techniques, twisting cytometry is most comparable to the pulling cytometry that we used in the current study. The upper bound values we obtained for SC cell modulus are a somewhat higher but comparable to the values measured on other endothelial cell types using the other techniques with the exception of the AFM measurements, which are mostly larger. This suggests that SC cells, in culture, do not have a unique elastic modulus as compared to other endothelial cell types.

We also estimated SC cell modulus in vivo. Interestingly, the in vivo values of modulus, at low IOP, are close to those estimated in culture. The in vivo results showed evidence of cellular stiffening at higher IOP values, although we should emphasize that the in vivo stiffness values derived in this work are only rough estimates. These results also suggested that SC cells cannot support a significant fraction of the pressure drop across the outflow system.

Certain limitations existed in this investigation. First, we made direct stiffness measurements only on cells in culture. SC cell in vivo are much thinner than in culture, and they are more variable in shape, perhaps due to the geometric complexity of Schlemm's canal compared to culture, coupled with the necessity of SC cells conforming to the shape of the Schlemm's canal in vivo. Another important difference is the absence of giant vacuoles and pores in SC cells in culture. We have also noted that inner wall cells have more peripheral actin in vivo than in culture (Read et al. 2007).

The substrate of cells in culture is also different than that of cells in vivo. We used our finite element model to examine the influence of substrate stiffness on the magnetic bead pulling measurements (data not shown). We found that for cells in culture thicker than 4 μm, substrate stiffness comparable or larger than the cell modulus had only a very minor effect. Modest effects on bead displacement (less than 25%) were seen for cells 2 or 3 μm in thickness. These findings suggest that the substrate did not significantly affect our measurements. However, we cannot rule out the possibility that substrate stiffness could have direct biological effects on cell modulus (Solon et al. 2007).

Finally, it is important to note that the in vitro experiments we conducted involved small deformations localized to the immediate vicinity of the magnetic bead. It is possible that the cells respond differently to such localized deformations as compared to large deformations of the entire cell (Humphrey 2002). Because of these differences, it was important to estimate the modulus of SC cells in vivo. These values, at low IOP, are close to those measured in culture, suggesting that the differences between in vivo and culture conditions may not play a major role in influencing the estimated modulus of the SC cells. However, the significant increase in our estimate of cell modulus in situ with increasing strain indicates that it is important to characterize the mechanical characteristics of these cells at physiological levels of strain. It would be beneficial to carry out future studies on the biomechanical characteristics of SC cells by quantifying whole-cell deformation under well-controlled conditions, e.g. through measurement of deformation of cultured SC cells subjected to a basal-to-apical pressure difference.

A bead is bound to a cell through focal contacts, but we modeled the contact as a surface to surface contact. More information on number and distribution of focal contacts between the bead and the cell, as well the strength of individual contacts, would be useful for improving the current model.

Attached beads were quite deeply immersed into the SC cells in some cases, with a mean measured half immersion angle of 84°. This is somewhat larger than the average of 67° measured on epithelial cells in a previous study (Laurent et al. 2002). One potential concern is that we were not able to directly measure immersion angles of the 4.5 μm magnetic beads, since these beads were not fluorescently labeled. Instead, we used 4 μm fluorescently labeled beads for this purpose. However, since both types of beads were functionalized with the same integrin-binding peptide (Peptite-2000), and the protocol for binding to the SC cells was nearly identical, the results of our fluorescently labeled bead experiments should be applicable to the magnetic beads.

We did not measure cell thickness at the bead location due to difficulties in resolving the basal cell surface, and instead performed parametric studies on cell thickness using finite element models. Bead displacement was found to be influenced by changes in cell thickness for cells less than 5 μm thick, but cell thickness had little influence for cells thicker than this (Fig. 11), in agreement with previous magnetic cytometry studies (Mijailovich et al. 2002; Karcher et al. 2003). Further studies should more closely examine cell thickness under beads bound to SC cells.

5 Conclusions

The combination of finite element modeling and magnetic bead pulling measurements is a viable approach for determining Young's modulus of elasticity of SC cells in culture. Our method for determining immersion angle can also be applied to magnetic twisting cytometry studies. The upper bound for the Young's modulus of the SC cells determined in our study ranged from 1,007–3,053 Pa in the central, non-nuclear regions, and was higher on the periphery and in the perinuclear regions. This is comparable but somewhat higher than the stiffness for other types of endothelial cells in culture. Using images from Grierson and Lee (1977), we were able to estimate that, at low IOP, SC cells in vivo appear to have stiffnesses similar to those in vitro, while at higher IOP, SC cells appear to stiffen significantly.

The modulus for SC cells that we have determined in this work can be used in modeling studies to determine the extent to which SC cells deform in response to the pressure drop across the inner wall endothelium. This in turn can be of use in making more precise estimates of the extent to which these cells can support a transmural pressure drop across this endothelium (Ethier et al. 2008). It will be particularly interesting to determine if the Young's moduli of SC cells from glaucomatous eyes differ from those of normal eyes.

Acknowledgments

References

Allingham RR, de Kater AW, Ethier CR, Anderson PJ, Hertzmark E, Epstein DL. The relationship between pore density and outflow facility in human eyes. Invest Ophthalmol Vis Sci. 1992; 33(5): 1661–1669. [PubMed: 1559766]

Alvarado JA, Alvarado RG, Yeh RF, Franse-Carman L, Marcellino GR, Brownstein MJ. A new insight into the cellular regulation of aqueous outflow:how trabecular meshwork endothelial cells drive a mechanism that regulates the permeability of Schlemm's canal endothelial cells. Br J Ophthalmol. 2005; 89(11):1500–1505.10.1136/bjo.2005.081307 [PubMed: 16234461]

Bausch AR, Ziemann F, Boulbitch AA, Jacobson K, Sackmann E. Local measurements of viscoelastic parameters of adherent cell surfaces by magnetic bead microrheometry. Biophys J. 1998; 75(4): 2038–2049.10.1016/S0006-3495(98)77646-5 [PubMed: 9746546]

Bill A, Svedbergh B. Scanning electron microscopic studies of the trabecular meshwork and the canal of Schlemm—an attempt to localize the main resistance to outflow of aqueous humor in man. Acta Ophthalmol (Copenh). 1972; 50:295–320. [PubMed: 4678226]

Braet F, Rotsch C, Wisse E, Radmacher M. Comparison of fixed and living liver endothelial cells by atomic force microscopy. Appl Phys A Mater Sci Process. 1998; 66:S575–S578.

Burke, A.; Roberts, B.; O'Brien, E.; Stamer, W. Effects of Na2EDTA and hydrostatic pressure on transendothelial electrical resistances and hydraulic conductivity of human Schlemm's canal monolayers. 2002. (in review)

Caille N, Thoumine O, Tardy Y, Meister JJ. Contribution of the nucleus to the mechanical properties of endothelial cells. J Biomech. 2002; 35(2):177–187.10.1016/S0021-9290(01)00201-9 [PubMed: 11784536]

Cheezum MK, Walker WF, Guilford WH. Quantitative comparison of algorithms for tracking single fluorescent particles. Biophys J. 2001; 81(4):2378–2388.10.1016/S0006-3495(01)75884-5 [PubMed: 11566807]

Costa KD, Sim AJ, Yin FC. Non-Hertzian approach to analyzing mechanical properties of endothelial cells probed by atomic force microscopy. J Biomech Eng. 2006; 128(2):176–184.10.1115/1.2165690 [PubMed: 16524328]

Deguchi S, Maeda K, Ohashi T, Sato M. Flow-induced hardening of endothelial nucleus as an intracellular stress-bearing organelle. J Biomech. 2005; 38(9):1751–1759.10.1016/j.jbiomech.2005.06.003 [PubMed: 16005465]

Ethier C, Read A, Chan D. Biomechanics of Schlemm's canal endothelial cells:influence on F-actin architecture. Biophys J. 2004; 87:2828–2837.10.1529/biophysj.103.038133 [PubMed: 15454474]

Ethier CR. The inner wall of Schlemm's canal (REVIEW). Exp Eye Res. 2002; 74:161–172.10.1006/exer.2002.1144 [PubMed: 11950226]

Ethier, CR.; Simmons, CA. Introductory biomechanics: from cells to organisms. Cambridge University Press; Cambridge: 2007.

Ethier, CR.; Zeng, D.; Read, AT.; Chan, D.; Gong, H.; Johnson, M. Pressure-induced deformation of Schlemm's canal endothelial cells. ARVO; Ft. Lauderdale: 2008.

Feneberg W, Aepfelbacher M, Sackmann E. Microviscoelasticity of the apical cell surface of human umbilical vein endothelial cells (HUVEC) within confluent monolayers. Biophys J. 2004; 87(2):1338–1350.10.1529/biophysj.103.037044 [PubMed: 15298936]

Ferko MC, Patterson BW, Butler PJ. High-resolution solid modeling of biological samples imaged with 3D fluorescence microscopy. Microsc Res Tech. 2006; 69(8):648–655.10.1002/jemt.20332 [PubMed: 16758474]

Fung, Y. A first course in continuum mechanics. Prentice-Hall Inc; Englewood Cliffs: 1977.

Gelles J, Schnapp B, Sheetz M. Tracking kinesin-driven movements with nanometre-scale precision. Nature. 1988; 331(4):450–453.10.1038/331450a0 [PubMed: 3123999]

Gilmont R. Measurement and control liquid—viscosity correlations for flowmeter catculations. Chem Eng Prog. 2002; 98(10):36–41.

Grierson I, Lee WR. Pressure-induced changes in the ultrastructure of the endothelium lining Schlemm's canal. Am J Ophthalmol. 1975; 80:863–884. [PubMed: 811121]

Grierson I, Lee WR. Light microscopic quantitaion of the endothelial vacuoles in Schlemm's canal. Am J Ophthalmol. 1977; 84:234–246. [PubMed: 407798]

Henon S, Lenormand G, Richert A, Gallet F. A new determination of the shear modulus of the human erythrocyte membrane using optical tweezers. Biophys J. 1999; 76(2):1145–1151.10.1016/S0006-3495(99)77279-6 [PubMed: 9916046]

Hogan, MJ.; Alvarado, JA.; Weddel, J. Histology of the human eye: an atlas and textbook. W.B. Saunders Co; Philadelphia: 1971.

Humphrey J. On mechanical modeling of dynamic changes in the structure and properties of adherent cells. Math Mech Solids. 2002; 7:521–539.10.1177/108128650200700504

Johnson M. What controls aqueous humour outflow resistance? Exp Eye Res. 2006; 82(4):545–557.10.1016/j.exer.2005.10.011 [PubMed: 16386733]

Johnson M, Chan D, Read T, Christensen C, Sit A, Ethier CR. The pore density in the inner wall endothelium of Schlemm's canal of glaucomatous eyes. Invest Ophthalmol Vis Sci. 2002; 43:2950–2955. [PubMed: 12202514]

Karcher H, Lammerding J, Huang H, Lee RT, Kamm RD, Kaazempur-Mofrad MR. A three-dimensional viscoelastic model for cell deformation with experimental verification. Biophys J. 2003; 85(5):3336–3349.10.1016/S0006-3495(03)74753-5 [PubMed: 14581235]

Karl MO, Fleischhauer JC, Stamer WD, Peterson-Yantorno K, Mitchell CH, Stone RA, Civan MM. Differential P1-purinergic modulation of human Schlemm's canal inner-wall cells. Am J Physiol Cell Physiol. 2005; 288(4):C784–C794.10.1152/ajpcell.00333.2004 [PubMed: 15590899]

Kass MA, Heuer DK, Higginbotham EJ, Johnson CA, Keltner JL, Miller JP, Parrish RK 2nd, Wilson MR, Gordon MO. The Ocular Hypertension Treatment Study: a randomized trial determines that topical ocular hypotensive medication delays or prevents the onset of primary open-angle glaucoma. Arch Ophthalmol. 2002; 120(6):701–713. see comment. discussion 829–30. [PubMed: 12049574]

Kataoka N, Iwaki K, Hashimoto K, Mochizuki S, Ogasawara Y, Sato M, Tsujioka K, Kajiya F. Measurements of endothelial cell-to-cell and cell-to-substrate gaps and micromechanical

properties of endothelial cells during monocyte adhesion. Proc Natl Acad Sci USA. 2002; 99(24): 15638–15643.10.1073/pnas.242590799 [PubMed: 12434019]

Laurent VM, Henon S, Planus E, Fodil R, Balland M, Isabey D, Gallet F. Assessment of mechanical properties of adherent living cells by bead micromanipulation: comparison of magnetic twisting cytometry vs optical tweezers. J Biomech Eng. 2002; 124(4):408–421.10.1115/1.1485285 [PubMed: 12188207]

Maepea O, Bill A. Pressures in the juxtacanalicular tissue and Schlemm's canal in monkeys. Exp Eye Res. 1992; 54(6):879–883.10.1016/0014-4835(92)90151-H [PubMed: 1521580]

Mathur AB, Collinsworth AM, Reichert WM, Kraus WE, Truskey GA. Endothelial, cardiac muscle and skeletal muscle exhibit different viscous and elastic properties as determined by atomic force microscopy. J Biomech. 2001; 34(12):1545–1553.10.1016/S0021-9290(01)00149-X [PubMed: 11716856]

Mathur AB, Reichert WM, Truskey GA. Flow and high affinity binding affect the elastic modulus of the nucleus, cell body and the stress fibers of endothelial cells. Ann Biomed Eng. 2007; 35(7): 1120–1130.10.1007/s10439-007-9288-8 [PubMed: 17385045]

Matthews BD, Overby DR, Alenghat FJ, Karavitis J, Numaguchi Y, Allen PG, Ingber DE. Mechanical properties of individual focal adhesions probed with a magnetic microneedle. Biochem Biophys Res Commun. 2004; 313(3):758–764.10.1016/j.bbrc.2003.12.005 [PubMed: 14697256]

Mijailovich SM, Kojic M, Zivkovic M, Fabry B, Fredberg JJ. a finite element model of cell deformation during magnetic bead twisting. J Appl Physiol. 2002; 93(4):1429–1436. [PubMed: 12235044]

Miyazaki H, Hayashi K. Atomic force microscopic measurement of the mechanical properties of intact endothelial cells in fresh arteries. Med Biol Eng Comput. 1999; 37(4):530–536.10.1007/ BF02513342 [PubMed: 10696714]

Oden, JT. Mechanics of elastic structures. McGraw-Hill; New York: 1967.

Ohayon J, Tracqui P. Computation of adherent cell elasticity for critical cell-bead geometry in magnetic twisting experiments. Ann Biomed Eng. 2005; 33(2):131–141.10.1007/ s10439-005-8972-9 [PubMed: 15771267]

Ohayon J, Tracqui P, Fodil R, Fereol S, Laurent VM, Planus E, Isabey D. Analysis of nonlinear responses of adherent epithelial cells probed by magnetic bead twisting: A finite element model based on a homogenization approach. J Biomech Eng. 2004; 126(6):685–698.10.1115/1.1824136 [PubMed: 15796327]

Overby DR, Matthews BD, Alsberg E, Ingber DE. Novel dynamic rheological behavior of individual focal adhesions measured within single cells using electromagnetic pulling cytometry. Acta Biomater. 2005; 1(3):295–303.10.1016/j.actbio.2005.02.003 [PubMed: 16701808]

Quigley HA, Broman AT. The number of people with glaucoma worldwide in 2010 and 2020. Br J Ophthalmol. 2006; 90(3):262–267. see comment. 10.1136/bjo.2005.081224 [PubMed: 16488940]

Read AT, Chan DW, Ethier CR. Actin structure in the outflow tract of normal and glaucomatous eyes. Exp Eye Res. 2007; 84(1):214–226.10.1016/j.exer.2005.10.035 [PubMed: 17219625]

Sato H, Kataoka N, Kajiya F, Katano M, Takigawa T, Masuda T. Kinetic study on the elastic change of vascular endothelial cells on collagen matrices by atomic force microscopy. Colloids Surf B Biointerfaces. 2004; 34(2):141–146.10.1016/j.colsurfb.2003.12.013 [PubMed: 15261083]

Sato M, Nagayama K, Kataoka N, Sasaki M, Hane K. Local mechanical properties measured by atomic force microscopy for cultured bovine endothelial cells exposed to shear stress. J Biomech. 2000; 33(1):127–135.10.1016/S0021-9290(99)00178-5 [PubMed: 10609525]

Sato M, Theret DP, Wheeler LT, Ohshima N, Nerem RM. Application of the micropipette technique to the measurement of cultured porcine aortic endothelial cell viscoelastic properties. J Biomech Eng. 1990; 112(3):263–268.10.1115/1.2891183 [PubMed: 2214707]

Schrot S, Weidenfeller C, Schaffer TE, Robenek H, Galla HJ. Influence of hydrocortisone on the mechanical properties of the cerebral endothelium in vitro. Biophys J. 2005; 89(6):3904–3910.10.1529/biophysj.104.058750 [PubMed: 16183884]

Solon J, Levental I, Sengupta K, Georges PC, Janmey PA. Fibroblast adaptation and stiffness matching to soft elastic substrates. Biophys J. 2007; 93(12):4453–4461.10.1529/biophysj. 106.101386 [PubMed: 18045965]

Stamer WD, Roberts BC, Howell DN, Epstein DL. Isolation, culture, and characterization of endothelial cells from Schlemm's canal. Invest Ophthalmol Vis Sci. 1998; 39(10):1804–1812. [PubMed: 9727403]

Theret DP, Levesque MJ, Sato M, Nerem RM, Wheeler LT. The application of a homogeneous half-space model in the analysis of endothelial cell micropipette measurements. J Biomech Eng. 1988; 110(3):190–199. [PubMed: 3172738]

Underwood JL, Murphy CG, Chen J, Franse-Carman L, Wood I, Epstein DL, Alvarado JA. Glucocorticoids regulate transendothelial fluid flow resistance and formation of intercellular junctions. Am J Physiol. 1999; 277(2 Pt 1):C330–C342. [PubMed: 10444410]

Wang N, Butler JP, Ingber DE. Mechanotransduction across the cell surface and through the cytoskeleton. Science. 1993; 260(5111):1124–1127.10.1126/science.7684161 [PubMed: 7684161]

Wang N, Ingber DE. Probing transmembrane mechanical coupling and cytomechanics using magnetic twisting cytometry. Biochem Cell Biol. 1995; 73(7–8):327–335. [PubMed: 8703406]

Yih, C. Fluid Mechanics: a concise introduction to the theory. West River Press; Ann Arbor: 1988.

Zeng, D.; Juzkiw, T.; Ethier, CR.; Johnson, M. Estimating Young's modulus of Schlemm's canal endothelial cells. ARVO; Ft. Lauder-dale: 2007.

TM = trabecular meshwork
SC = Schlemm's canal
JCT = juxtacanalicular tissue
IW = inner wall
OW = outer wall
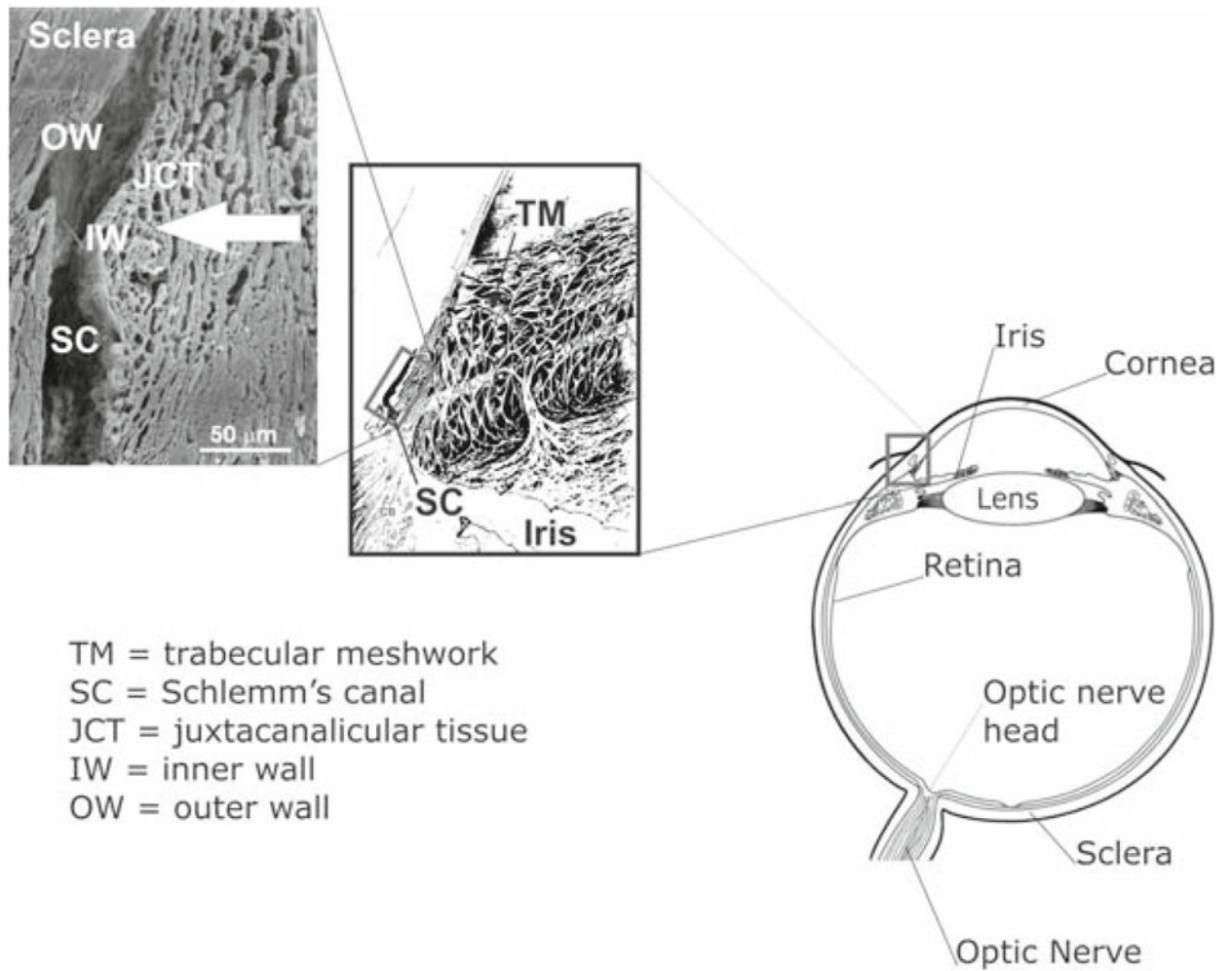
Fig. 1.
Overview of ocular anatomy in aqueous humor drainage. Reproduced from Ethier et al. (2004) with permission of Elsevier. *Middle* panel modified from Hogan et al. (1971) with permission of Elsevier
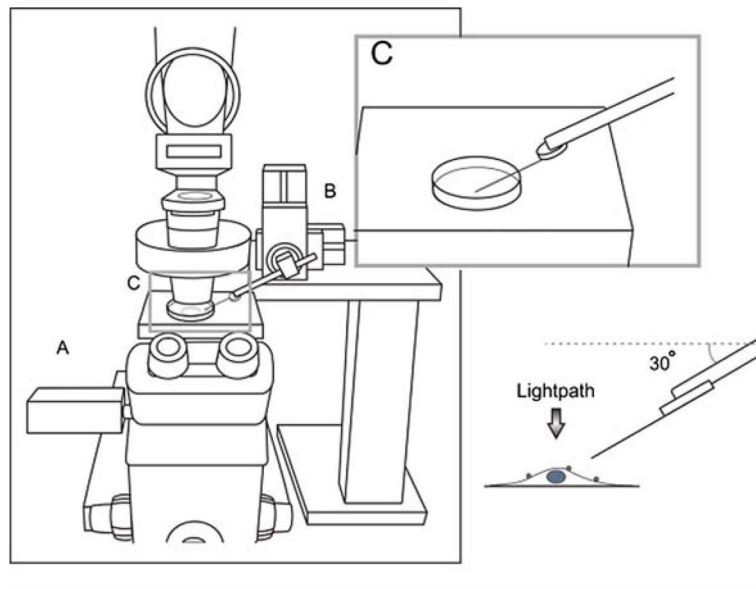
Fig. 2.
Inverted motorized microscope with bead-pulling setup including video camera (*A*), electric micromanipulator (*B*) and magnetic microneedle assembly; *inset* shows details of (*C*) with cell culture
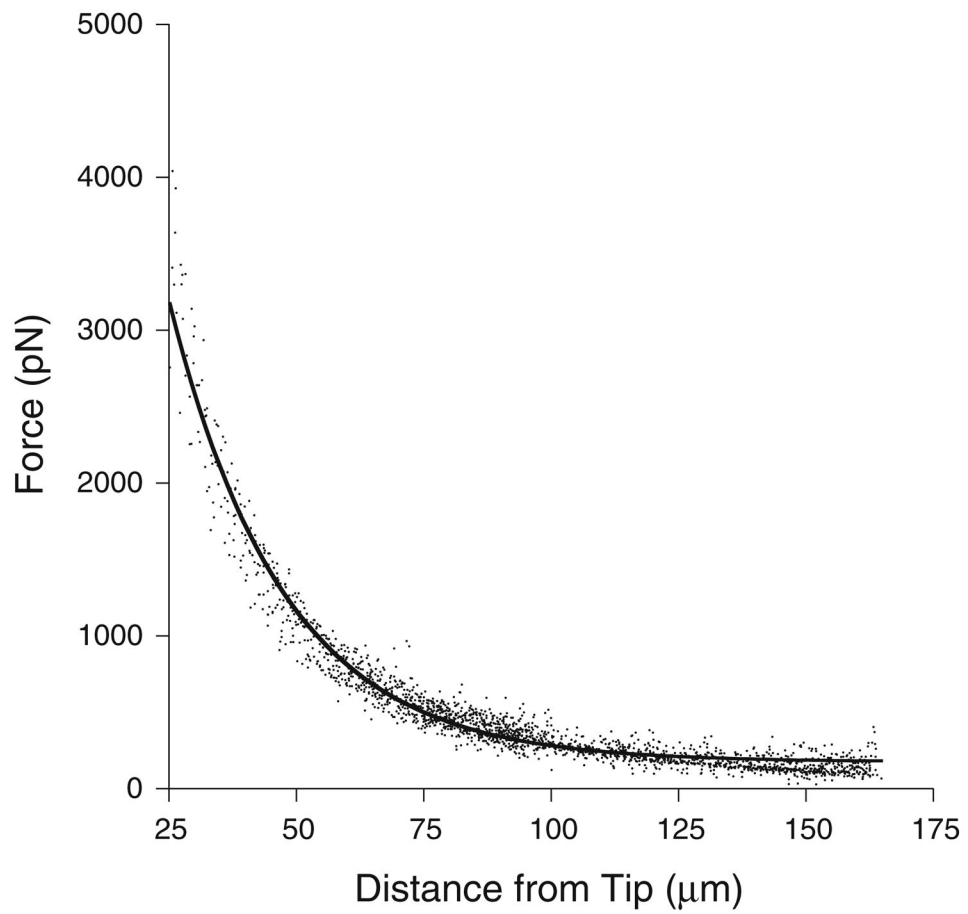
Fig. 3.
Horizontal magnetic force on bead as a function of distance from the tip of the microneedle.
Solid line is best exponential fit
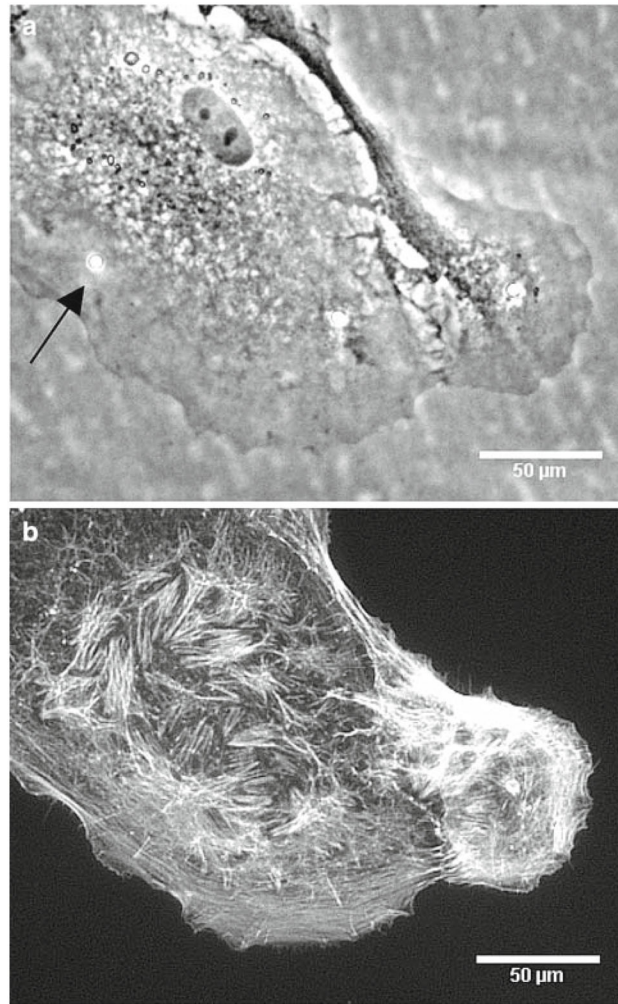
Fig. 4.
a Phase contrast image of an SC cell with a bead (*black arrow*) attached to it. **b** fluorescence microscopy image of same cell showing actin labeling with rhodamine-phalloidin (Alexa Fluor 546, Molecular Probes). Note that there may be a second cell immediately adjacent to the cell of interest in this image
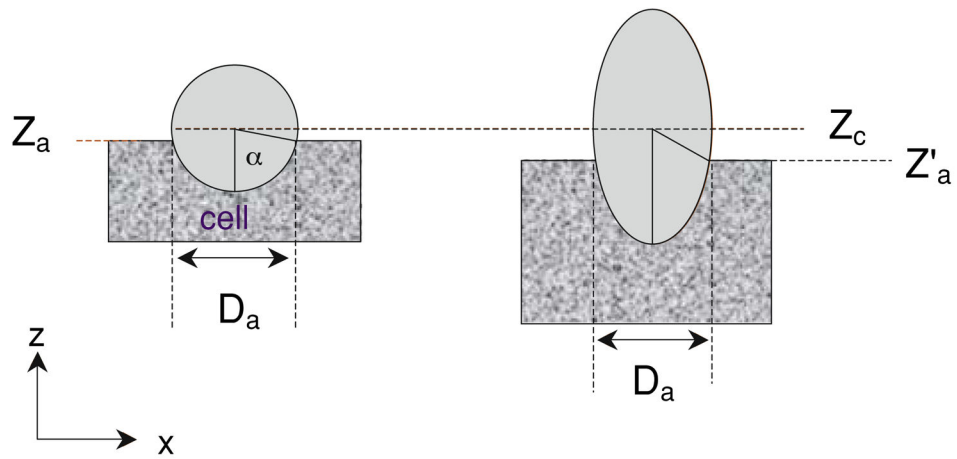
Fig. 5.
The *left* panel shows a schematic of an $x – z$ plane of a bead partially embedded in a cell, while the *right* panel shows the axially distorted view of this bead as imaged by confocal microscopy. α is the half immersion angle. D_a is the section diameter of the bead. z_c and z_a are the z-coordinates of the bead center and the apical surface of the cell, respectively, while z_a' is the distorted z-coordinate of the apical surface of the cell
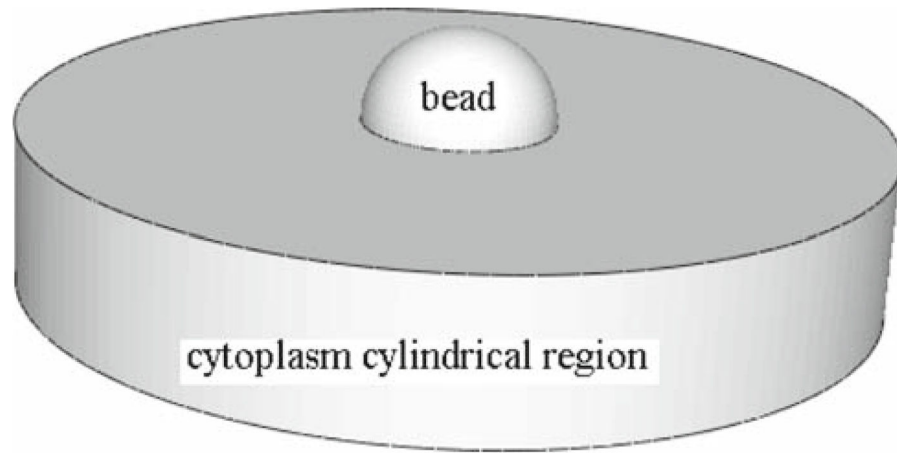
Fig. 6.
Domain used in finite element modeling showing a bead embedded in a cylindrical region of cytoplasm with a radius of 10 μm. In this model shown, the half-immersion angle is 98°
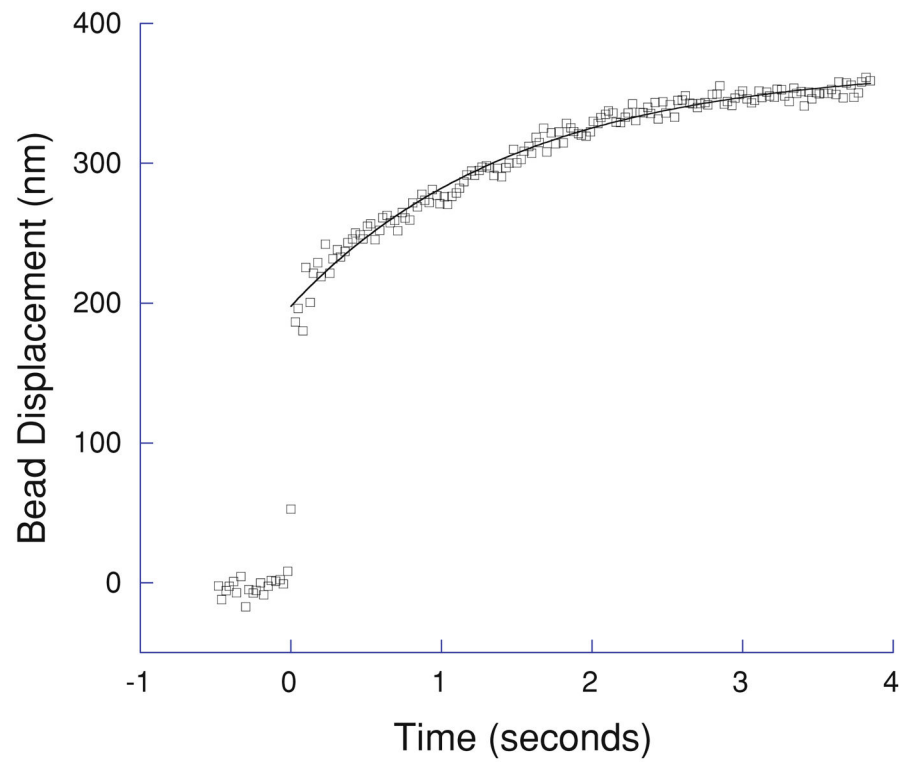
Fig. 7.
Displacement (*squares*) of the bead attached to cell 2 resulting from magnetic pulling,
initiated at time zero. The *line* is a best fit to these data for times >0 using Eq. (2). The initial
bead displacement due to the pulling is approximately 200 nm, corresponding to the elastic
response of the cell to the pulling. This is typical of the response of the beads due to
magnetic pulling
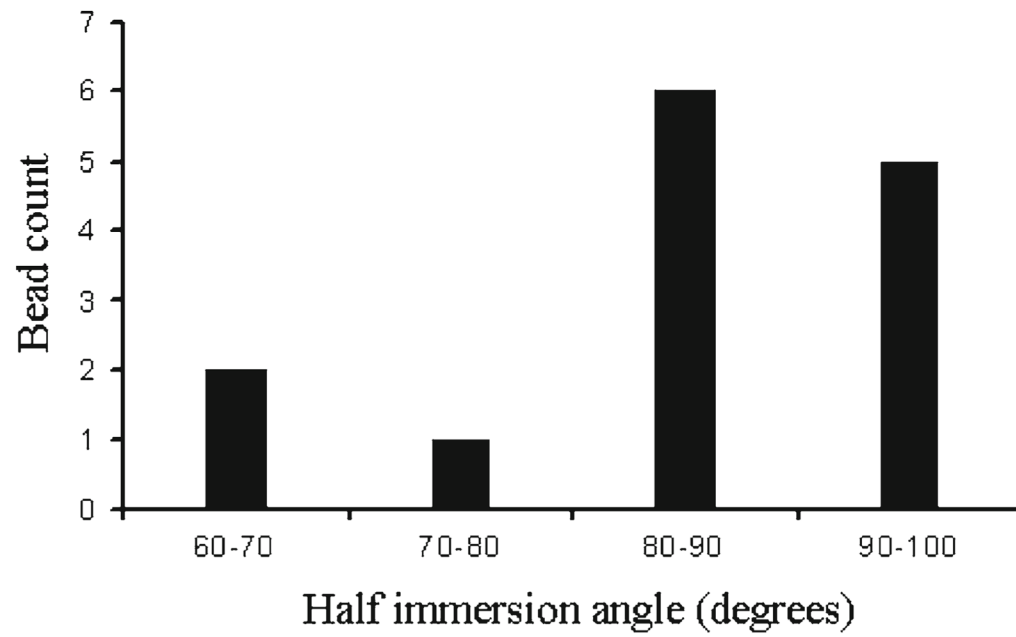
Fig. 8.
Spectrum of half-immersion angles measured from fourteen 4 μm fluorescent beads attached to SC cells. The beads selected for the measurement were at least 10 μm from the edge of the cell, and were not in the nuclear region
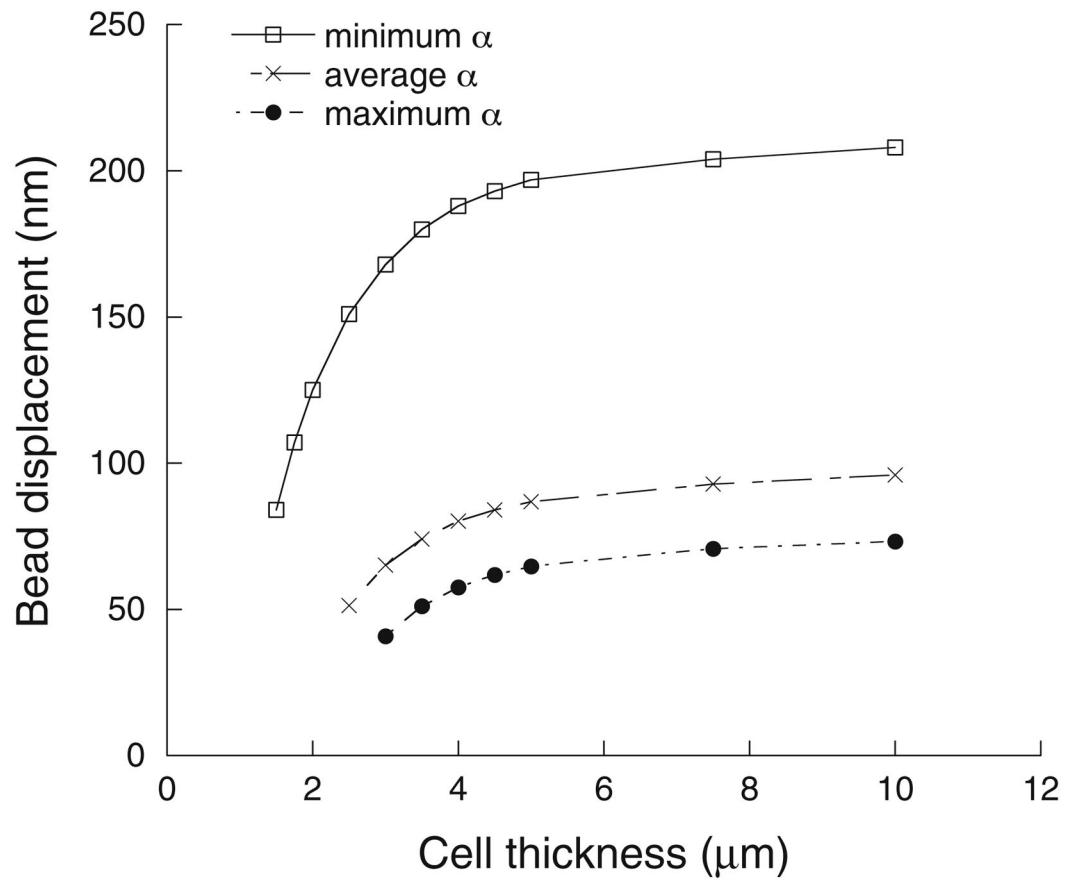
Fig. 9.
Results of parametric studies on cell thickness, showing computed bead displacements as a function of cell thickness. The half immersion angles (a) were 60°, 84°, and 98°, corresponding to the minimum, average and maximum measured values, respectively. Young's modulus of the cell was assumed to be 1,000 Pa. Lines shown are best fit to the equation $s = A - Be^{-w/C}$, where w is cell thickness, s is bead displacement and A, B and C are fitting constants
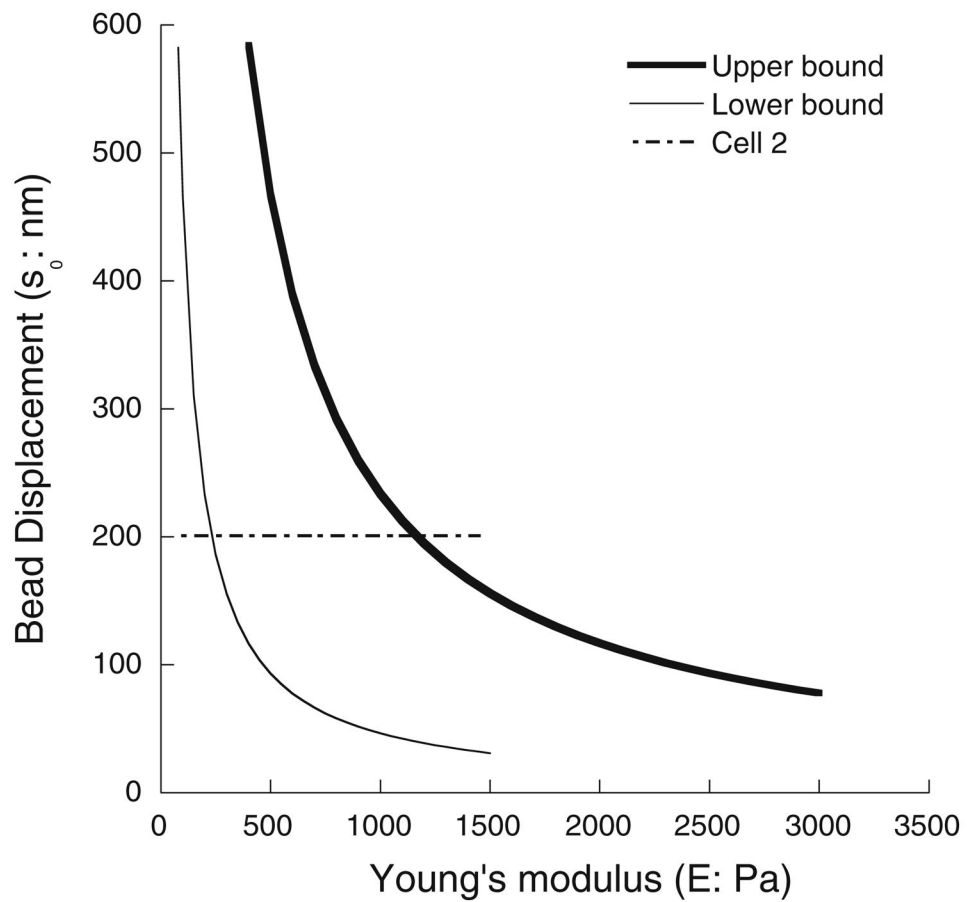
Fig. 10.
Results of parametric studies showing how computed initial bead displacement (s_0) varies with the Young's modulus of the cell (E, in Pa), for both the upper and lower bound cases. The initial displacement (s_0) of cell 2 measured from bead pulling experiment is also indicated in the figure (*horizontal line*). From this measured displacement, we deduce an upper bound and lower bound on E for this cell. See text for definition of upper and lower bound cases
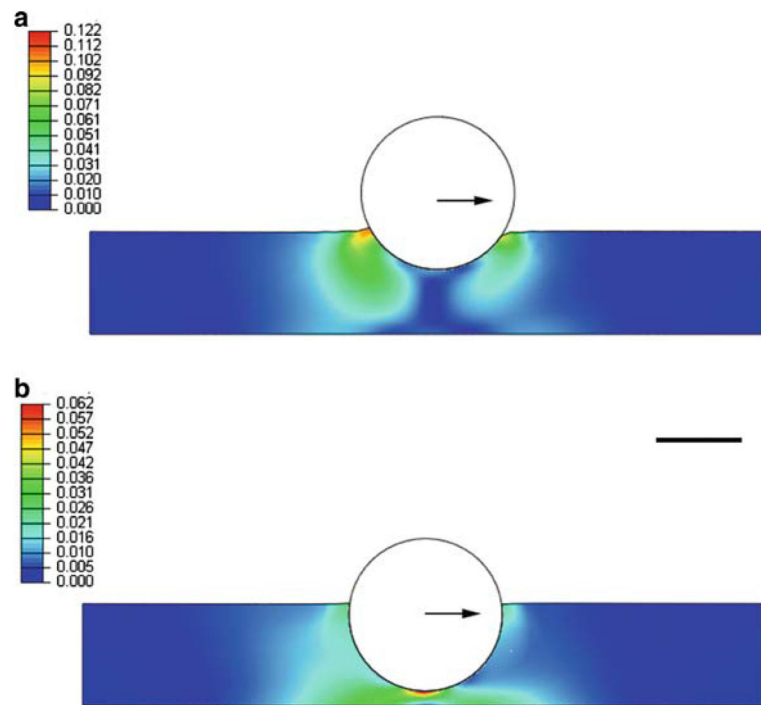
Fig. 11.
Section view of the computed strain field (maximum principal strain) around the bead for the minimum half immersion angle (60°, **a**) and the maximum half immersion angle (98°, **b**). *Black arrows* indicate the direction of pulling force in this section. The section plane passes through the bead center, and is perpendicular to the cell surface. Cell thickness is 3 μm, and the Young's modulus is 1,000 Pa. The *scale bar* in **b** is 3 μm in length
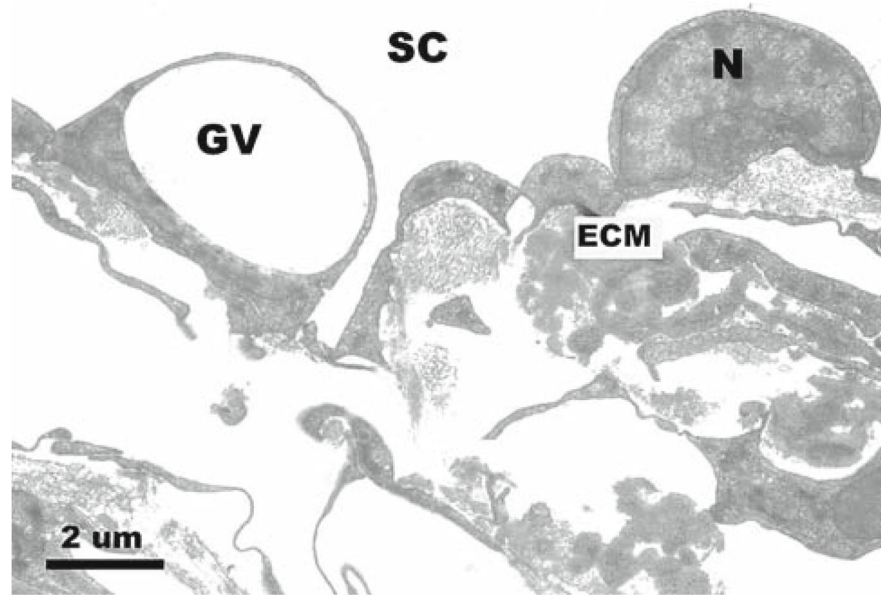
Fig. 12.
Inner wall of Schlemm's canal of enucleated human eye perfused at 8 mm Hg. *GV* giant vacuole; *SC* Schlemm's canal; *ECM* extracellular matrix; *N* cell nuclei. Reproduced from Ethier (2002) with permission of Elsevier

Table 1

Initial (s_0) and long-time displacements (s_∞) of beads that were (A) bound in the central, non-nuclear regions, (B) bound near the nucleus or (C) bound near the periphery of the cell

Bead	s_0 (μm)	SE	s_∞ (μm)	SE	τ_0 (s)	SE	E_0, lower bound (Pa)	E_0, upper bound (Pa)	E_∞, lower bound (Pa)	E_∞, upper bound (Pa)	Bead position
1	232	3	313	2	1.30	0.12	201	1,007	149	747	A
2	201	2	370	2	1.48	0.06	232	1,165	126	632	A
3	173	3	308	3	1.23	0.09	269	1,350	151	759	A
4	157	5	539	6	1.80	0.07	297	1,489	86	434	A
5	77	2	179	2	1.08	0.07	609	3,053	260	1,306	A
6	59	2	143	2	1.42	0.12	790	3,961	326	1,634	B
7	32	3	120	4	2.02	0.19	1,456	7,303	388	1,948	B
8	29	4	282	4	1.97	0.08	1,607	8,059	165	829	B
9	147	7	327	9	2.08	0.23	317	1,590	142	715	C
10	97	2	214	2	1.05	0.049	480	2,409	218	1,092	C
11	50	4	225	5	2.35	0.14	932	4,674	207	1,039	C
12	32	2	75	2	0.85	0.14	1,456	7,303	621	3,116	C

τ_0 is the time constant (see Eq. 2) and SE is standard error of the measurement. Bounds on cell moduli, E_0 and E_∞, are based on upon s_0, and s_∞, respectively, and determined as described in the text

Table 2

Young's modulus of elasticity measured through a variety of experimental techniques on different types of endothelial cells

Source	Cell type	Experimental method	Young's modulus (Pa)
Costa et al. (2006)	Human aortic endothelial cell	AFM	1,000–5,000
Schrot et al. (2005)	Porcine/murine cerebral capillary endothelial cells	AFM	5,000
Sato et al. (2004)	Human umbilical vein endothelial cell	AFM	5,000–10,000
Mathur et al. (2001)	Human umbilical vein endothelial cell	AFM	1,400 (near edge); 6,800 (over nucleus); 3,300 (in between)
Sato et al. (2000)	Bovine aortic endothelial cell	AFM	1,000–7,000
Miyazaki and Hayashi (1999)	Rabbit aortic endothelial cell	AFM	600–10,000
Braet et al. (1998)	Rat liver endothelial cell	AFM	2,000
Feneberg et al. (2004)	Human umbilical vein endothelial cell	Magnetic twisting cytometry	400
Deguchi et al. (2005)	Bovine thoracic aortic endothelial cell	Micropipette aspiration	400 (nucleus)
Sato et al. (1990))	Porcine aortic endothelial cell	Micropipette aspiration	150
Theret et al. (1988)	Bovine aortic endothelial cell	Micropipette aspiration	300–800
Caille et al. (2002)	Bovine aortic endothelial cell	Compression between microplates	300–700 (cytoplasm); 4,000–8,000 (nucleus)

AFM atomic force microscopy

Table 3

Estimated modulus of primate SC cells based on vacuolar volume as determined by Grierson and Lee (1977)

IOP (mm Hg)	E (Pa)			
	$P = 10\%$ of total pressure drop		$P = 100\%$ of total pressure drop	
	Constant wall δ	Constant wall V	Constant wall δ	Constant wall V
8–15	1,722	3,922	17,220	39,220
15–22	4,541	20,908	45,410	209,080
22–30	8,004	74,165	80,040	741,650

See text for details. δ thickness, V volume